SARTORIUS

One Tool to Retrieve Them All

Simplifying Progress

Fully automated and uniquely versatile cell imaging and retrieval system to simplify your antibody, rare-cell and stem-cell research.

With CellCelector Flex, you have everything you need for imaging, screening, retrieving and verifying target cells in one place.

It's an all-in-one solution that reduces steps, streamlines workflows, and accelerates processing - while capturing cells without damage and enabling incredibly high viability.

Learn More About CellCelector

SARTORIUS

ARTICLE

BIOTECHNOLOGY BIOENGINEERING WILEY

Experimental k_S estimation: A comparison of methods for *Corynebacterium glutamicum* from lab to microfluidic scale

Heiko Steinhoff[1,2] | Maurice Finger[3] | Michael Osthege[4,5] | Corinna Golze[1] | Simone Schito[5] | Stephan Noack[5] | Jochen Büchs[3] | Alexander Grünberger[1,2,6]

[1]Multiscale Bioengineering, Bielefeld University, Bielefeld, Germany

[2]Center for Biotechnology (CeBiTec), Bielefeld, Germany

[3]AVT – Biochemical Engineering, RWTH Aachen University, Aachen, Germany

[4]Institute of Biotechnology, RWTH Aachen University, Aachen, Germany

[5]Institute of Bio- and Geoscience, IBG-1: Biotechnology, Jülich, Germany

[6]Microsystems in Bioprocess Engineering, Institute of Process Engineering in Life Sciences, Karlsruhe Institute of Technology, Karlsruhe, Germany

Correspondence

Alexander Grünberger, Microsystems in Bioprocess Engineering, Institute of Process Engineering in Life Sciences, Karlsruhe Institute of Technology, 76131 Karlsruhe, Germany.
Email: alexander.gruenberger@kit.edu

Abstract

Knowledge about the specific affinity of whole cells toward a substrate, commonly referred to as k_S, is a crucial parameter for characterizing growth within bioreactors. State-of-the-art methodologies measure either uptake or consumption rates at different initial substrate concentrations. Alternatively, cell dry weight or respiratory data like online oxygen and carbon dioxide transfer rates can be used to estimate k_S. In this work, a recently developed substrate-limited microfluidic single-cell cultivation (sl-MSCC) method is applied for the estimation of k_S values under defined environmental conditions. This method is benchmarked with two alternative microtiter plate methods, namely high-frequency biomass measurement (HFB) and substrate-limited respiratory activity monitoring (sl-RA). As a model system, the substrate affinity k_S of *Corynebacterium glutamicum* ATCC 13032 regarding glucose was investigated assuming a Monod-type growth response. A k_S of <70.7 mg/L (with 95% probability) with HFB, 8.55 ± 1.38 mg/L with sl-RA, and 2.66 ± 0.99 mg/L with sl-MSCC was obtained. Whereas HFB and sl-RA are suitable for a fast initial k_S estimation, sl-MSCC allows an affinity estimation by determining t_D at concentrations less or equal to the k_S value. Thus, sl-MSCC lays the foundation for strain-specific k_S estimations under defined environmental conditions with additional insights into cell-to-cell heterogeneity.

KEYWORDS

affinity constant, cell-to-cell heterogeneity, *Corynebacterium glutamicum*, microfluidic single-cell cultivation, Monod growth kinetics, respiratory activity monitoring

1 | INTRODUCTION

The growth rate μ is one central parameter for the characterization, comparison, and classification of cellular processes. To predict microbial growth behavior, Monod (1949) established the first growth kinetic model in 1949 while considering the bioavailability of the substrate (Equation 1). Within this empirical relationship, k_S denotes the affinity of a bacterium toward a corresponding substrate S with the concentration c_s and marks the concentration, where half of the specific maximum growth rate μ_{max} is reached (Ferenci, 1999).

$$\mu = \mu_{max} \cdot \frac{c_S}{c_S + k_S}. \tag{1}$$

The growth of cells in bioprocesses is affected by biological, chemical, and physical factors (Takors, 2012). In large-scale bioreactors, gradients of the substrate, dissolved gases, and pH occur through limiting capacities of engines, resulting in reduced input of power per volume, increased mixing times, and reduced $k_L a$ values (Bylund et al., 1998; Enfors et al., 2001; Junker, 2004; Mandenius, 2016). Hence, if the consumption rates of components required by the cells are higher than their supply, limiting conditions are present. This can lead to stress responses, which have a substantial impact on the yield and quality of the target product (Enfors et al., 2001). Therefore, access to precise k_S values is urgently required to model complex substrate gradients occurring within bioreactors by computational fluid dynamics. Additionally, k_S values are necessary to adjust the steady-state concentration of a carbon source, especially in bioprocesses operated in chemostat mode, to secure an efficient conversion of substrate into biomass (Harrison, 1973).

State-of-the-art estimation of k_S is based on measuring specific substrate uptake rates q_S within the exponential growth phase (Kell & Sonnleitner, 1995). Uptake rates q_S are determined as a function of substrate concentration c_S and correspond to the ratio of growth rate μ to the biomass yield $Y_{X/S}$ in accordance with Equation (2). This lays the foundation to estimate k_S by incorporating the Monod expression (Equation 1) and rearranging for k_S (Equation 3) (Schmideder et al., 2015). The approach can be extended for chemostat cultivations under the condition that no residual concentration is present in the effluent by replacing the substrate concentration c_S with the feed concentration $c_{S,feed}$, as well as the growth rate with the set dilution rate D (Equation 4) (Graf et al., 2020).

$$q_S = \frac{\mu}{Y_{X/S}}, \tag{2}$$

$$k_S = c_S \cdot \left(\frac{\mu_{max}}{q_S \cdot Y_{X/S}} - 1 \right), \tag{3}$$

$$k_S = c_{S,feed} \cdot \left(\frac{\mu_{max}}{D} - 1 \right). \tag{4}$$

Mainly three methods are reported in the literature to determine uptake rates q_S, including high-performance liquid chromatography (HPLC) (Senn et al., 1994), enzymatic assays (Graf et al., 2020), or liquid scintillation counting (Lindner et al., 2011). However, liquid scintillation counting is only applicable if a labeled substrate such as ^{14}C glucose is used. Alternative approaches to estimate the k_S value are to measure the oxygen uptake rate (OUR) or the oxygen transfer rate (OTR) of aerobic growing cells, which correlates to growth (Stöckmann et al., 2003; Wechselberger et al., 2013). With the biomass concentration c_X and the biomass yield on oxygen $Y_{X/O2}$, the k_S can be estimated according to the following equation:

$$k_S = c_S \cdot \left(\frac{\mu_{max} \cdot c_X}{OUR \cdot Y_{X/O_2}} - 1 \right). \tag{5}$$

Respirometry methods for the estimation of kinetic parameters have been used more frequently and can deliver similarly precise k_S estimations in comparison to established chemostat methods (Legan & Owens, 1987; Oliveira et al., 2009). These methods often rely on experiments in a respirometer but can also be conducted in situ through pulse respirometry (Goudar & Strevett, 1998; Ordaz et al., 2008).

Reported k_S values are scarce even for prominently used organisms. *Corynebacterium glutamicum* is recognized as a model organism in bioprocess engineering and industrial microbiology for its broad capabilities as a producer of value-added goods like amino acids (Hermann, 2003), organic acids (Wendisch et al., 2006), polymer precursors (Becker et al., 2018), aromatic chemicals (Wendisch et al., 2016), and proteins (Freudl, 2017). Moreover, *C. glutamicum* stands out for its robustness in large-scale applications (Graf et al., 2020; Vertès et al., 2012). However, even for this industrial-relevant organism, only a few published k_S values are available regarding glucose (Graf et al., 2020; Lindner et al., 2011; Uhde et al., 2013). As stated by Kovárová-Kovar and Egli, this is due to the fact, of analytical difficulty in monitoring substrates at growth-controlling concentrations (Kovárová-Kovar & Egli, 1998). The applied state-of-the-art methods for a high precision k_S estimation are technically very complex, and even though they primarily provide merely extrapolated values, if liquid scintillation counting was not used.

This study demonstrates a microfluidic method and compares this method to two microtiter plate methods for estimating k_S values using *C. glutamicum* ATCC 13032 as a model organism to expand the biochemical engineering toolbox. For all methods, a Monod-type response of the specific growth rate is assumed to estimate k_S. The first microtiter plate method is based on a computational approach for uncertainty quantification and relies on high-frequency biomass observations (HFB). This is accomplished with an end-to-end Bayesian modeling approach, according to Helleckes et al. (2022). The second method utilizes the newly developed micro(µ)-scale Transfer rate Online Measurement (µTOM) (Dinger et al., 2022) device for high-throughput respiratory activity measurements. Substrate-limited respiratory activity (sl-RA) monitoring determines the change in the OTR after spiking a defined glucose concentration, which correlates for aerobic growing cells with the growth rate. These microtiter plate methods are compared with the substrate-limited microfluidic single-cell cultivation (sl-MSCC) method. Novel microfluidic single-cell cultivations (MSCC) allow the cultivation of cells in defined environments (Wang et al., 2010), which can be maintained even for substrate-limiting conditions (Lindemann et al., 2019). This technology was applied to estimate the k_S value of *C. glutamicum* ATCC 13032 regarding protocatechuate acid (PCA) as a carbon source (Lindemann et al., 2019). Burmeister et al. (2021) used the same approach and estimated the lysine affinity for the lysine auxotrophic *C. glutamicum* ΔlysA pEKEx2-eYFP strain. However, MSCC as a technology has not yet been systematically established as a tool for k_S estimation. It is unclear how comparable results are to conventionally established methods since studies on main carbon sources like glucose have not been performed to date. Finally, presented technologies (HFB,

sl-RA, and sl-MSCC) are compared with literature values and future application fields of each individual method are pointed out.

2 | MATERIALS AND METHODS

2.1 | Bacterial strain growth media

The bacterial strain *C. glutamicum* ATCC 13032 was used in this study. Cultivations were performed with modified CGXII medium (Unthan et al., 2014), containing per liter of distilled water 20 g $(NH_4)_2SO_4$, 1 g K_2HPO_4, 1 g KH_2PO_4, 5 g urea, 13.25 mg $CaCl_2·2H_2O$, 0.25 g $MgSO_4·7H_2O$, 10 mg $FeSO_4·7H_2O$, 10 mg $MnSO_4·H_2O$, 0.02 mg $NiCl_2·6H_2O$, 0.313 mg $CuSO_4·5H_2O$, 1 mg $ZnSO_4·7H_2O$, 0.2 mg biotin, 37.5 mg citrate, 42 g MOPS, and 40 g D-glucose, unless stated otherwise. Similar to previous studies, PCA was replaced by citrate as iron chelator (Ho et al., 2022). Citrate as a potential available carbon source can only be metabolized by *C. glutamicum* if the saline concentration of NaCl is at least 1 g/L (Liebl et al., 1989; von der Osten et al., 1989).

2.2 | High-frequency biomass observations and Bayesian Monod modeling

Microtiter plate batch cultivation experiments were carried out in a 48-well FlowerPlate (m2p-labs GmbH) incubated in a BioLector Pro (m2p-labs GmbH) (Figure 1a). Culture well A01 was inoculated to an initial biomass concentration of 0.25 g/L from a glycerol stock. The cultivation parameters were set to 1400 rpm, 85% humidity, and 30 °C. The online signals for biomass (backscatter; gain 3), dissolved oxygen pO_2 and pH were measured with a cycle time set to 1 min (Figure 1b). Detailed information on reference gain and filterset can be found in the raw data file online (Osthege & Schito, 2022). The FlowerPlate was covered with a gas-permeable sealing foil (m2p-labs GmbH) to prevent contamination and allow uniform gas exchange. Medium preparation and inoculation were performed manually under a laminar flow hood.

Raw data was parsed with bletl version 1.1.0 (Osthege, Tenhaef, Helleckes, et al., 2022; Osthege, Tenhaef, Zyla, et al., 2022). Backscatter observations between 2 and 9.5 h were removed from
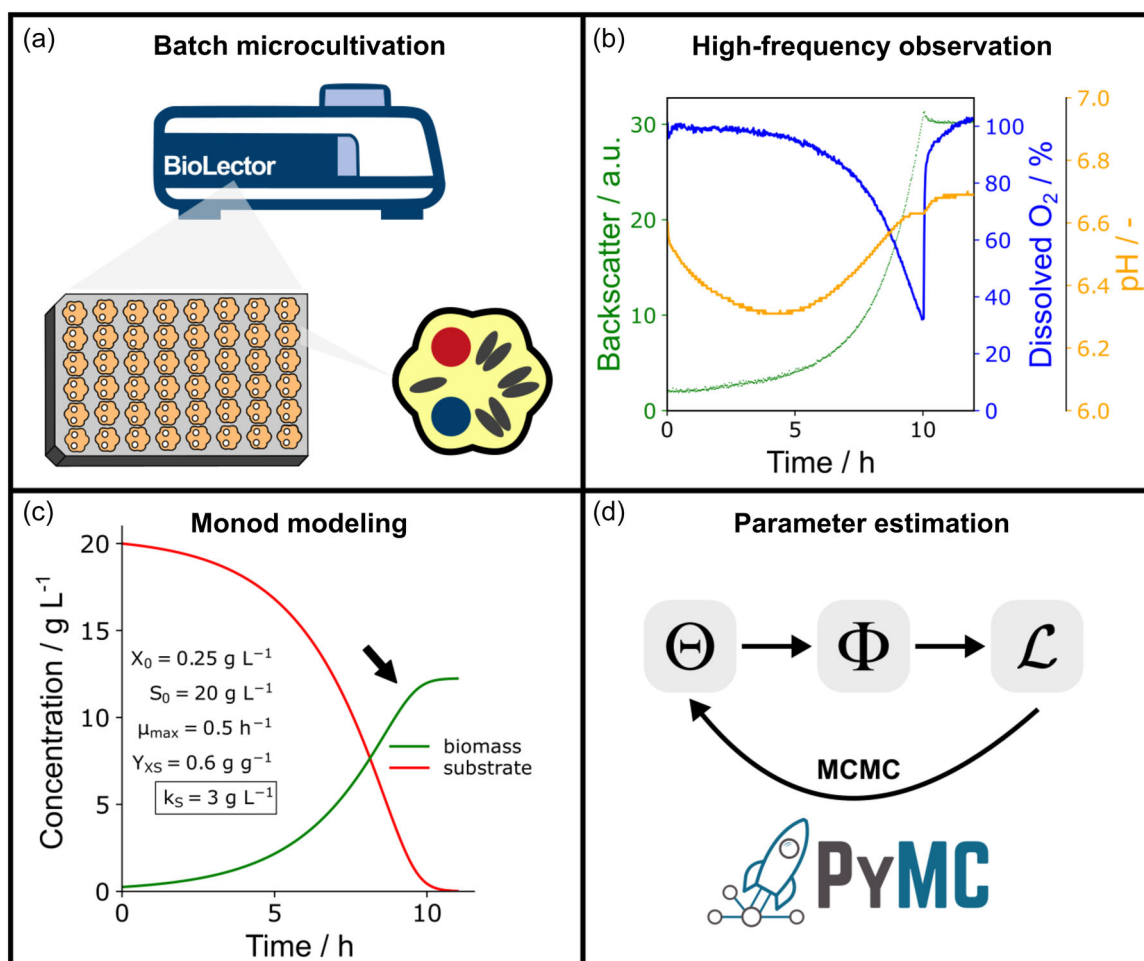

FIGURE 1 Experimental setup and workflow for estimating the k_S of microbial cells with high-frequency biomass observations. (a) Microbioreactor batch cultivations with (b) high-frequency measurements of biomass-related backscatter. The k_S parameter in the (c) Monod model causes curvature (arrow) of the biomass trajectory. A computational model Φ predicts the likelihood $\mathcal{L}$ of observations. (d) Probabilistic parameter estimation obtained by Markov-chain Monte Carlo (MCMC) using the probabilistic programming library PyMC.

the data set to account for inaccuracies of the Monod assumption of approximately constant growth rate (Equation 1 with $c_S \gg k_S$) for most of the exponential phase (Helleckes et al., 2022; Osthege, Tenhaef, Zyla, et al., 2022; Unthan et al., 2014). A biomass/backscatter calibration was established from reference backscatter measurements of a robotically prepared biomass dilution series of 48 biomass concentrations ranging from 23.1 ± 0.4 g/L to a 1000x dilution. The calibration model built with calibr8 version 6.5.2 (Osthege & Helleckes, 2022a) and the parameter estimates as well as a visualization of the fit, can be found in the supporting information.

A Monod differential equation model was set up to describe the time series of biomass concentrations in the batch cultivation (Figure 1c). The respective equations and explanations are given in Chapter 3.1. The calibration model was used to relate predicted biomass concentrations with observed backscatter values, creating a likelihood for parameter estimation (Figure 1d). The model was implemented as a probabilistic model using Python packages PyMC version 4.0.0b6 (Wiecki et al., 2022) and murefi version 5.1.0 (Osthege & Helleckes, 2022b). Bayesian parameter estimation was performed by sampling the joint posterior probability distribution of model parameters using PyMC. In this iterative procedure, thousands of parameter sets are used to predict biomass trajectories with the ODE model and accepted or rejected based on the prior probability of the parameter values and how likely it would have been to observe the given data from such a trajectory. The result is a collection of thousands of parameter sets for the Monod model, each of which could plausibly explain the observed data. A detailed description of the method is given by Helleckes et al. (2022).

Here, the PyMC implementation of the DE-MCMC-Z algorithm (ter Braak & Vrugt, 2008) was used with 20,000 tuning and 50,000 draw iterations in four independent Markov chains. Convergence of the Markov-chain Monte Carlo (MCMC)-sampling was checked by validating that all $\hat{R} < 1.01$ using ArviZ version 0.12.0 (O. Martin et al., 2021). For detailed explanations of calibration modeling and the Bayesian modeling of batch cultivations using the Monod model, it can be referred to Helleckes et al. (2022). The full data set and code to reproduce the k_S analysis using the high-resolution biomass and Bayesian ODE modeling approach are provided online (Osthege & Schito, 2022).

2.3 | Substrate-limited respiratory activity monitoring

For the respiratory determination of k_S, deep-well microtiter plates Riplate RW (Ritter GmbH) with 96 wells were used. The OTR of every well was online monitored with the µTOM (Figure 2a) (Dinger et al., 2022). All wells were filled with 1 mL of inoculated culture. Cultivations were performed at a temperature of 30°C, a shaking speed of 800 rpm, and a shaking diameter of 3 mm. Precultures for inoculation were performed in 250 mL shake flasks with CGXII medium with 10 g/L glucose as the sole carbon source. The main culture was inoculated with 5 (v/v)% from a stationary phase preculture and was also conducted in CGXII medium but with 1 g/L glucose.

After the initial batch cultivations, 100 µL glucose solutions with different concentrations were spiked into each well of the microtiter plate (Figure 2b). This resulted in a theoretical filling volume of 1.1 mL per well with final glucose concentrations of 0.0, 2.5, 5.0, 7.5, 10.0, 12.5, 15.0, 17.5, 20.0, 30.0, 40.0, 50.0, 60.0, 70.0, 80.0 100.0 mg/L. A multichannel multistepper pipette Eppendorf Research pro (Eppendorf) was used to spike all wells 2 min before the next OTR measurement phase started. The first 30 s of the measurement phase of the µTOM device were cutoff, and OTRs were determined by the oxygen partial pressure decrease within the next 2 min. The end of the initial batch and glucose depletion was indicated by a rapid decrease in the OTRs (Figure 2c), whereas the glucose spike resulted in a concentration-dependent fast increase of the OTR. The resulting OTRs after the spike with 0.0 mg/L of glucose were subtracted from all other resulting OTRs. A regression of these values to the Monod equation was performed with OriginPro (OriginPro 2020 9.7.0.188; OriginLab Corporation) to estimate the k_S value (Figure 2d).

2.4 | Substrate-limited microfluidic single-cell cultivation

2.4.1 | Design and microfluidic chip fabrication

The design of the microfluidic chip is based on a recently developed MSCC method from Lindemann et al. (2019). The MSCC systems consist of 12 arrays of "quasi" one-dimensional growth channels to restrict cell proliferation of a few cells (<15) along one axis (Figure 3a). These growth channels are open on both ends and connected to adjacent supply channels. There, the fresh medium flows with a high velocity to ensure a constant and defined medium supply to the growth channels. In total, one cultivation unit consists of 1440 growth channels.

A silicon wafer mold was fabricated with a two-layer photolithography process and served as a mold for PDMS (poly(dimethylsiloxane)) soft lithography (Grünberger et al., 2013). The construction and development of a siliconwafer was carried out according to the protocol of Täuber et al. (2020). During soft lithography, the siliconwafer was covered with PDMS in a ratio 10:1 between the base and curing agent (Sylgard 184 Silicone Elastomer, Dow Corning Corporation). Afterward, the wafer was degassed in a desiccator for 30 min and backed at 80 °C for 2 h (universal cupboard; Memmert GmbH). After this step, the PDMS chips were cut out from the wafer, cleaned three times with isopropanol, and blown dry with pressurized air. The cover glasses (D 263 T eco, $39.5 \times 34.5 \times 0.175$ mm, Schott) for the microfluidic chip were also cleaned after the same protocol. Afterward, the PDMS chip and the cover glass were activated with O_2 plasma (Femto Plasma Cleaner; Diener Electronics) for 24 s with a power of 45% and assembled. Before the use, PDMS-glass bonding was strengthened by a 2 min bake at 80 °C.
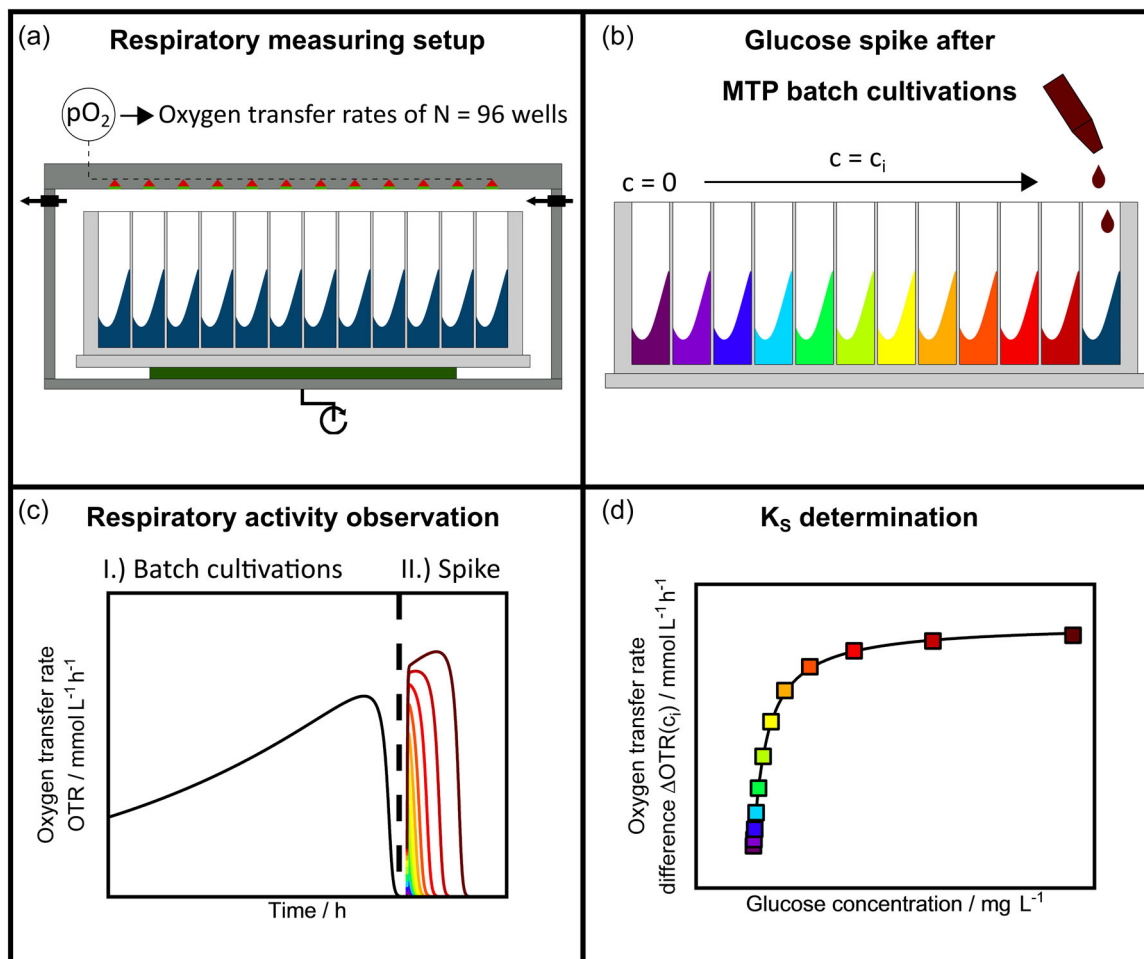
FIGURE 2 Experimental setup and workflow for estimating the k_S of microbial cells with substrate-limited respiratory activity monitoring. (a) Micro(μ)-scale Transfer rate Online Measurement device (μTOM) for 96-deepwell microtiter plates. The figure for the μTOM device was adapted from Dinger et al. (2022). (b) Spike of varying substrate concentrations after the termination of the batch cultivations with 96 replicates. (c) Observation of the substrate-dependent oxygen transfer rates. (d) k_S determination based on Monod-type respiratory response.

2.4.2 | Single-cell cultivation

Overnight precultures of *C. glutamicum* were inoculated from glycerol stock in 10 mL CGXII medium in 100 mL flasks on a rotary shaker at 120 rpm. Cells from the overnight culture were transferred to inoculate a second shake flask culture with a starting OD_{600} of 0.1 for harvesting of cells in the exponential growth phase. The cells were used to inoculate the microfluidic device manually through a syringe containing a cell suspension with an OD of approximately 0.6. Seeding of the growth channels was obtained by random trapping of cells. After successfully seeding, the microfluidic chip was connected to pressure-driven pumps (Flow EZ Pressure Controller; Fluigent) and controlled by software (All in One; Fluigent). An inlet pressure of 150 mbar was applied for a constant medium supply (Figure 3b) (Li et al., 2017). Afterward, growth kinetic studies in CGXII were performed containing concentrations from 0 up to 150 g/L glucose. The possibility of interactions between hydrophilic molecules such as glucose and PDMS as a hydrophobic polymer can be excluded (Toepke & Beebe, 2006). Each cultivation medium

was additionally sterile filtered to prevent channel clogging during microfluidic experiments.

2.4.3 | Live cell imaging, data analysis, and growth rate modeling

Time-lapse microscopy was performed using an inverted automated microscope from Nikon (Nikon Eclipse Ti2; Nikon). The microscope stage was surrounded with a cage incubator for optimal temperature control (Cage incubator; OKO Touch; Okolab S.R.L.). The microfluidic device was placed inside the cage incubator in an in-house fabricated chip holder. Additionally, the setup was equipped with a 100x oil objective (CFI P-Apo DM Lambda 100x Oil; Nikon GmbH), DS-Qi2 camera (Nikon camera DS-Qi2; Nikon GmbH), and an automated focus system (Nikon PFS; Nikon GmbH) to compensate the thermal drift during long term microscopy (Figure 3a). For each experiment, 80 positions containing several cultivation channels were selected manually and were managed with NIS-Elements Imaging Software
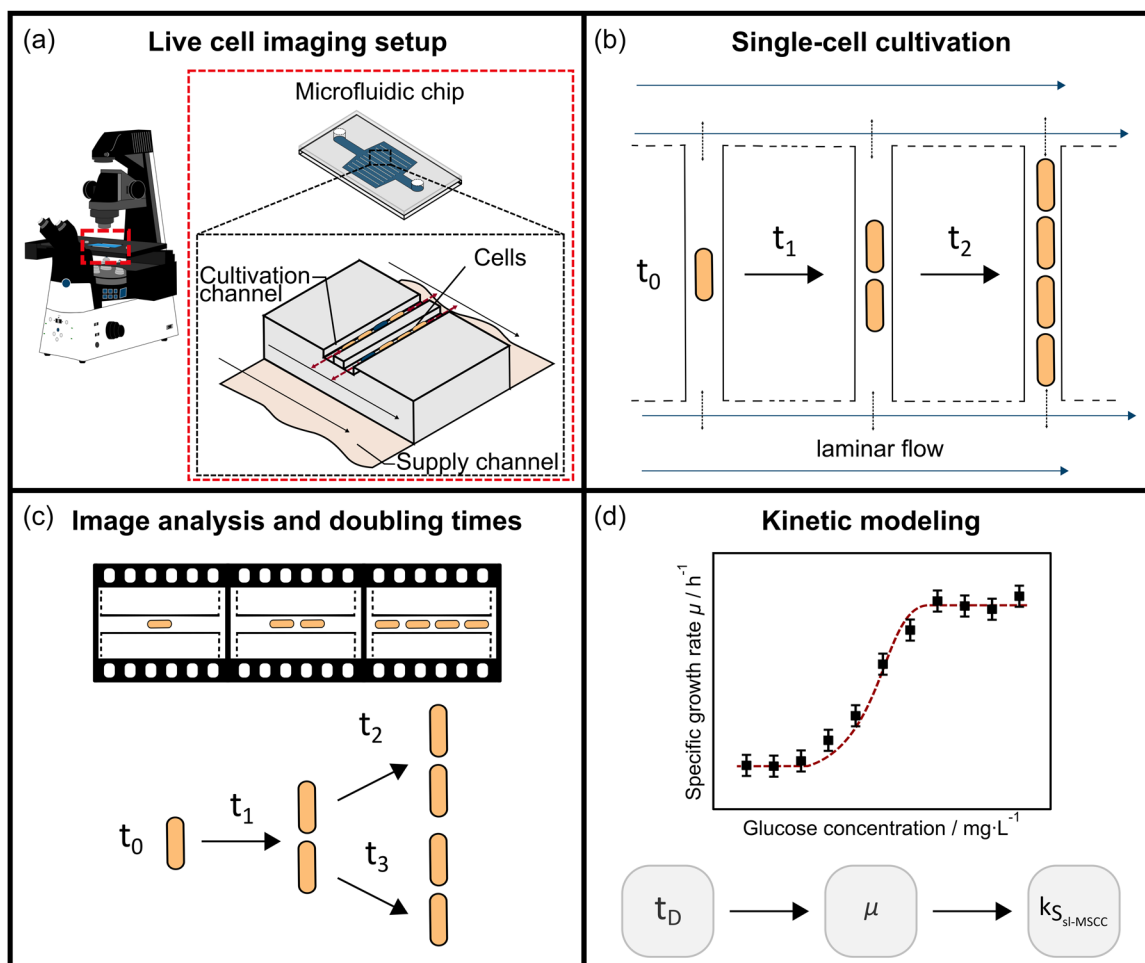
FIGURE 3 Experimental setup and workflow for estimating the k_S of microbial cells with substrate-limited microfluidic single-cell cultivation (sl-MSCC). (a) Live cell imaging setup consisting of an inverted phase-contrast microscope and a microfluidic single-cell cultivation chip, allowing high-spatiotemporal resolution. (b) Single-cell cultivation performed under varying substrate concentrations. (c) Determination of t_D of the online-monitored time-lapse data. (d) Establishing a kinetic model based on a Monod-type response by the conversion of t_D into growth rates μ to display growth as a function of glucose concentration to estimate $k_{S,sl-MSCC}$.

(Nikon NIS Elements AR software package; Nikon GmbH). Time-lapse images were recorded every 5 min.

Data analysis of the live-cell image sequences was performed using the open-source software Fiji 1.52 (Schindelin et al., 2012). For determining single-cell division events, one offspring cell was selected whose descendants were present until the end of the measurement. Based on the growth of this cell line, it can usually be guaranteed that at least 50 single-cell division events occurred. Two categories were differentiated for the case that a selected glucose concentration resulted in reduced growth. The first category describes cell growth for less than four generations, defined as no growth. The second category describes cases where less than 50 single-cell division events were observed. In this case, offspring of further descendants were considered for quantification to reach the minimum of at least 50 single-cell division events.

The doubling time of each offspring of the selected cell lineage was determined after the first division event through selection of the cell by using the integrated multipoint function of Fiji (Figure 3c).

This ensured a frame-independent tracking of temporally asymmetric divisions of daughter cells depending on the generation time. The respective mean values for t_D and growth rates were determined using the geometric mean (Phoenix, 1997). Here, extreme outliers with $t_D > 1000$ min or $t_D < 30$ min were not considered, because the formula for the determination of the standard deviation uses summation of squared errors. Therefore, the impact of extreme outliers is espicalliy high for low sample sizes. We observed that doubling times of 1000 min or below 30 min generate a standard deviation equal to the mean. To avoid this, we neglected these extreme rare outliers when considiering our kinetics due to the loq frequency to determine an affinity reflecting more than 95% of the population. The first step in determining k_S is calculating the growth rate with each determined doubling time. The equation and explanation are stated in Chapter 3.1. Then, the corresponding geometric mean, including the standard deviation, is plotted as a function of the respective glucose concentration. A Monod kinetic fit is then established using OriginPro (OriginPro 2020 9.7.0.188;

OriginLab Corporation) (Figure 3d). The regression slope obtained from the logarithmic plot corresponds to k_S.

3 | RESULTS AND DISCUSSION

3.1 | Comparison of methodologies

In this work, three unique methods for k_S estimation are presented: HFB, sl-RA, and sl-MSCC. All methods assume a Monod-type growth response (Equation 1). Thereby, the k_S value is always estimated by observing the growth under substrate limiting conditions. For the understanding of the different methodologies and their potentials as well as limits, a comparison is given regarding (1) cultivation workflows, (2) computational approaches for k_S estimation, and (3) analytical procedures.

3.1.1 | Cultivation workflows

HFB and sl-RA are based on microtiter cultivation systems (Figures 1 and 2). In contrast, sl-MSCC is based on MSCC devices (Figure 3). In the HFB workflow, the biomass is observed during a batch cultivation over time. The glucose is steadily consumed by the cells until complete glucose consumption, which is indicated by a sharp rise in the DO (Figure 1b). The rise in DO can be attributed to the fact that the glucose uptake rate is linked via growth to the OUR. The link of growth and OUR is utilized for k_S estimation with sl-RA. For the sl-RA, depletion of glucose after an initial batch cultivation is indicated by a drop in OTR (Figure 2c). In comparison to the HFB workflow, after the termination of the batch cultivation, different glucose solutions are spiked into the microtiter plate wells to adjust defined substrate levels. For the third alternative, sl-MSCC, defined and contrasting to the other methods, constant conditions are reached by perfusion with a medium containing a defined glucose concentration. Thereof, HFB and sl-RA are faster and easier to perform. Nonetheless, sl-MSCC provides a more defined environment due to perfusion and thereby, constant substrate concentrations even at limiting conditions. In contrast to sl-MSCC and sl-RA, where glucose concentrations are set by perfusion or spiking, the glucose concentration is only measured once at the onset of the stationary phase with a hexokinase assay for the HFB.

3.1.2 | Computational approaches for k_S estimation

In HFB, a batch cultivation is monitored by backscatter measurements. For parameter inference, the parameter sets proposed by the MCMC algorithm are used to simulate biomass concentration trajectories using the differential model (Equation 6) based on the Monod equation (Equations 1 and 2). These concentration values are fed into an asymmetric logistic calibration model to predict the distribution of backscatter observations. This enables the model to relate model parameters with observations, learning about how well a chosen parameter set describes the data. For a detailed explanation of this modeling procedure, see Helleckes & Osthege et al. (2022).

$$\frac{dc_X}{dt} = \mu_{max} \cdot c_X \cdot \frac{c_S}{k_S + c_S},$$
$$\frac{dc_S}{dt} = \frac{-1}{Y_{X/S}} \cdot \frac{dc_X}{dt}. \tag{6}$$

Instead of the biomass concentration c_X, the OTR is observed in sl-RA. The change in dissolved oxygen dO_L/dt is assumed to be negligible compared with the OUR, similar to Mühlmann et al. (2018) and Ihling et al. (2021). Hence, the OTR is used equivalently to the OUR (Equation 7). Data by Graf et al. (2020) indicate a linear correlation of growth rates (0.2–0.4 h^{-1}) and OURs and therefore, a constant $Y_{X/O2}$. However, this assumption is not necessarily true at very low growth rates. Only due to this simplified linearity assumption of the growth rate and the OTR, the sl-RA model is interchangeable with the models of the other methods. Thereby, the k_S value can be estimated directly with the glucose concentration-dependent OTR and using a regression of the Monod equation.

$$OTR = OUR$$

$$\text{s. t. } OUR \gg \frac{dO_L}{dt}, \tag{7}$$

$$\mu = \frac{OTR \cdot Y_{X/O2}}{c_X}. \tag{8}$$

For sl-MSCC, single-cell doubling times t_D are determined. Under the assumption that both cells have the same size after splitting, the growth rate μ can be calculated (Equation 9). Similar to sl-RA, a mathematical fit under the assumption of Monod-type response of growth is used to estimate the k_S value based on the glucose concentration-dependent growth rates.

$$\mu = \frac{\ln 2}{t_D}. \tag{9}$$

3.1.3 | Analytical procedures

As a Mond-type growth response is assumed for all methods, the following analytical procedures are chosen to measure parameters correlating to the growth of *C. glutamicum*. For HFB, backscatter measurements are performed in a BioLector. In contrast, sl-MSCC allows single-cell tracking by inverted phase contrast microscopy. The sl-RA depends on the indirect growth tracking by monitoring the OTR. To this end, high-throughput OTR measurements are conducted in a µTOM device. The equipment for the presented methods is not available in every laboratory. However, the proposed approaches can be adapted for other devices and provide insight into the theoretical backgrounds behind k_S estimation.

3.2 | Substrate affinity k_S estimations

The HFB method for k_S estimation takes the data from the microbioreactor batch cultivation, comprised of 464 backscatter observations after preprocessing and one simulated glucose measurement. Parametrization of the probabilistic Monod model was obtained with uninformative prior beliefs of the model parameters: $S_0 \sim LogNormal(\mu = \log(20\frac{g}{L}), \sigma = 0.1)$, $X_0 \sim LogNormal(\mu = \log(0.25\frac{g}{L}), \sigma = 0.1)$, $\mu_{max} \sim Beta(\mu = 0.4, \sigma = 0.1)$, $Y_{X/S} \sim Beta(\mu = 0.6, \sigma = 0.05)$, $k_S \sim Uniform(0, \infty)$. Note that the prior information for k_S constrains it to positive numbers but does not bias the model beyond that.

The MCMC sampling of the joint posterior probability distribution (Figure 4b) for these five parameters given the 119 + 1 observations and corresponding calibration models yielded a total of 200,000 parameter vectors, each corresponding to one possible trajectory of Monod kinetics. In Figure 4c,d, individual examples of such trajectories are drawn alongside a density band representing the posterior probability distribution of trajectories. Vertical violin plots show the 90% highest-density intervals of the posterior probability distributions of biomass (green) and substrate (blue) concentrations obtained from single measurements with the calibration model. These are the narrowest intervals containing the inferred parameter (here: biomass concentration) with a probability of 90%. Note that inferences from single backscatter observations resulted in much
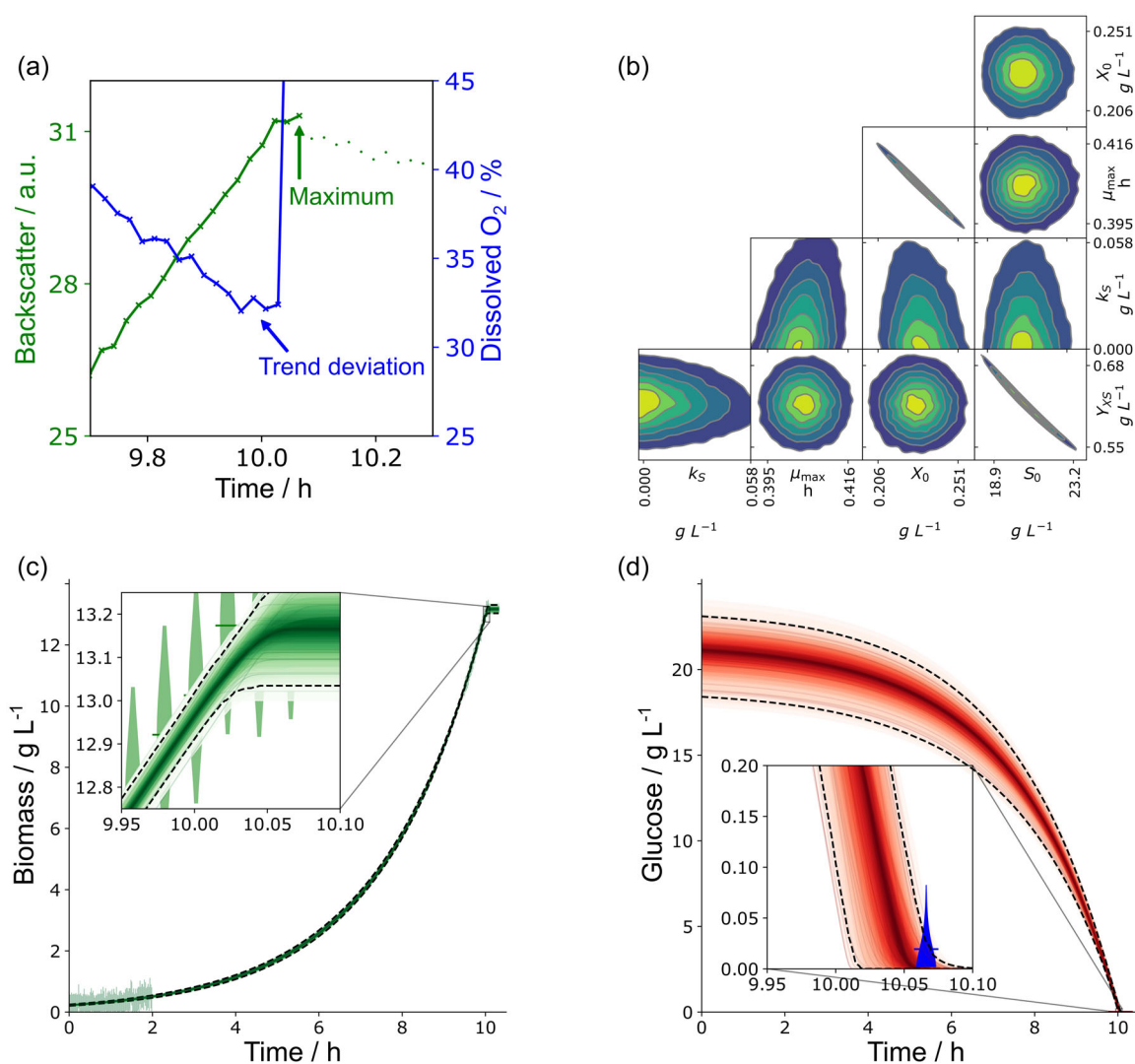

FIGURE 4 Monod modeling results for high-frequency biomass observations (HFB). In (a) the raw backscatter and DO observations of the transition from exponential to stationary phase show a deviation from the declining DO trend for three cycles (approx. 3 min) before a sharp rise in DO. (b) Data up to the first cycle after the rise was considered to infer posterior probabilities of the Monod model parameters. The $Y_{X/S}$ and S_0 as well as μ_{max} and X_0 parameters are strongly correlated. The highest probability density for the k_S parameter is near 0 mg/L. (c and d) Show the resulting distribution of biomass and substrate trajectories predicted from sampled parameter sets. Violins indicate the probabilities inferred from individual data points without the use of the Monod model. Thin lines indicate trajectories resulting from exemplary parameter sets. The dashed line indicates the highest density interval, around 90% of the probability mass.

—WILEY—

larger uncertainty about biomass concentration than those obtained from ODE model trajectories (green bands, dashed lines). This is because ODE trajectories are constrained by the relatively rigid assumption of Monod-like growth and the combined information from 119 observations. Nevertheless, the curvature of trajectories is visible at timescales of approximately less than 1 min (Figure 4c,d). This asymmetric observation of "less than" corresponds to the marginal posterior distribution of k_S exhibiting no lower tail toward 0 g/L, but a clear tail toward higher concentrations. In this case, 95% of the k_S posterior probability distribution is <70.7 mg/L, corresponding to the interpretation that k_S < 70.7 mg/L with a 95% probability according to this analysis. Since the 95% probability threshold is arbitrary, equally valid statements with slightly different interpretations can be provided: k_S < 21.5 mg/L with a 50% chance (the median) or k_S < 10.0 mg/L with a 26.4% chance.

In Figure 4b, two-dimensional marginals of the five-dimensional joint probability distribution are shown as kernel density estimates. These visualizations show that with this data set, k_S is not correlated to other parameters of the Monod model, whereas μ_{max} is strongly correlated with X_0, and $Y_{X/S}$ is strongly correlated with S_0. These correlations are structural and well expected (Helleckes et al., 2022). If a lower S_0 is estimated, Y_{XS} has to be higher to fit the biomass observations. Due to the strong Monod assumptions and the 464 backscatter observations, our posterior estimate for the μ_{max} of this batch is rather narrow with 90% of the probability mass in the interval [0.395, 0.416] h^{-1}.

For respiratory estimation of the k_S with the sl-RA, 96 batch cultivations were performed simultaneously in a 96-deepwell plate. The online monitored OTR of these cultivations show an increase and, therefore, the initial growth of *C. glutamicum* for the first 3 h (Figure 5a). The rapid decrease of the OTR afterwards points to the depletion of the main carbon source glucose, which was only supplied with 1 g/L. The utilization of alternative carbon sources leads to a low

OTR of around 1 mmol/L/h, which is also progressively decreasing after 3.5 h (Figure 5a). As soon as glucose is spiked into the wells, growth, according to Monod (Equation 1), sets in. Only for the glucose spike concentration of 0 mg/L a lower OTR after spiking was measured with 0.9 ± 0.1 mmol/L/h. The glucose-dependent OTRs are also depicted in Supporting Information: S14–16. The differences between the OTR reference value at 0 mg/L and all other OTRs were calculated (Figure 5b). For spiked glucose concentrations of at least 20 mg/L, a constant ΔOTR of 2 mmol/L/h is noticeable. The decreased ΔOTR value for the condition with a glucose concentration of 100 mg/L could be subject to measurement variance or caused by a physiological explanation due to overflow metabolism. However, as this work focuses on the k_S value, this trend was not further investigated here. For glucose concentrations of 20 to 0 mg/L, the ΔOTR is decreasing. With the regression to the Monod equation, a k_S of 8.55 ± 1.38 mg/L was obtained with a coefficient of determination of $R^2 = 0.95$. A logarithmic plot of Figure 5b is given in Supporting Information: S17.

Growth experiments in CGXII with varying glucose concentrations were performed with *C. glutamicum* at 30 °C using sl-MSCC for 72 h. For the assurance that the distribution of the doubling time follows a Gaussian distribution, distributions of selected concentrations are shown as examples. At glucose concentrations of 500 mg/L (Figure 6a), the average doubling time is about 75 ± 15 min with low variance. Furthermore, the single-cell t_D are normal distributed with a coefficient of determination of $R^2 = 0.97$. At glucose limiting concentrations, the dispersion and variance increase drastically, leading to t_D at 5 mg/L of 188 ± 204 min (Figure 6b) and at 2.5 mg/L of 122 ± 69 min (Figure 6c) with a coefficient of determination of $R^2 = 0.76$ and $R^2 = 0.89$, respectively. We exclude technical bias at the concentration of 5 mg/L due to limitations or gradients in nutrition. Thus, we are convinced that the nongaussian distribution is due to the limiting carbon-conditions itself. We speculate that the
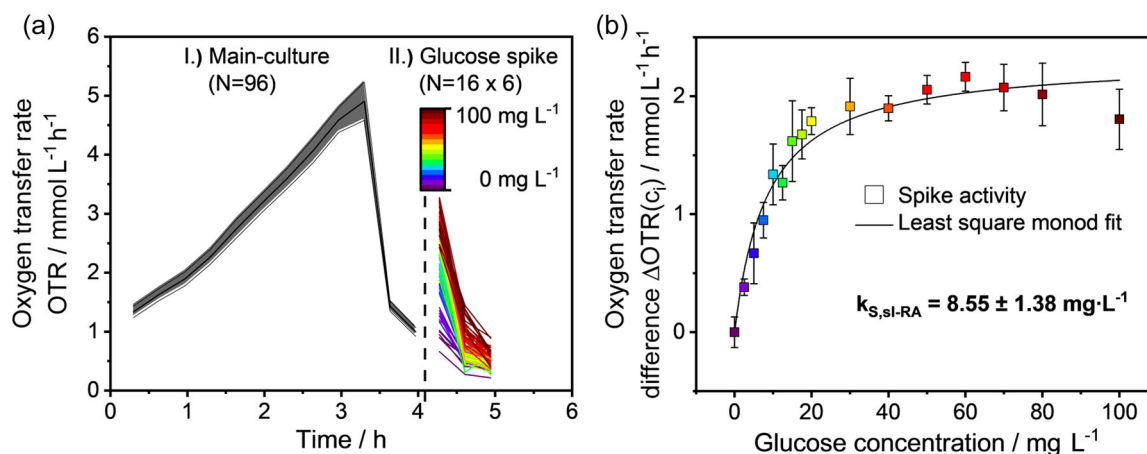

FIGURE 5 Substrate limited respiratory activity estimation (sl-RA) of the k_S for *Corynebacterium glutamicum* with glucose spiked batch cultivations. (a) Oxygen transfer rates of *C. glutamicum* cultivations (N = 96) spiked with 16 different glucose concentrations (N = 6) after glucose depletion of the main culture. (b) Correlation of the resulting oxygen transfer rate difference after the spike to the respective glucose concentrations with N = 6. Culture conditions: 96-deepwell microtiter plate, V_L = 1 mL, n = 800 rpm, d_0 = 3 mm, T = 30 °C, CGXII medium without protocatechuate acid, spike with 100 μL of 16 different glucose concentrations.
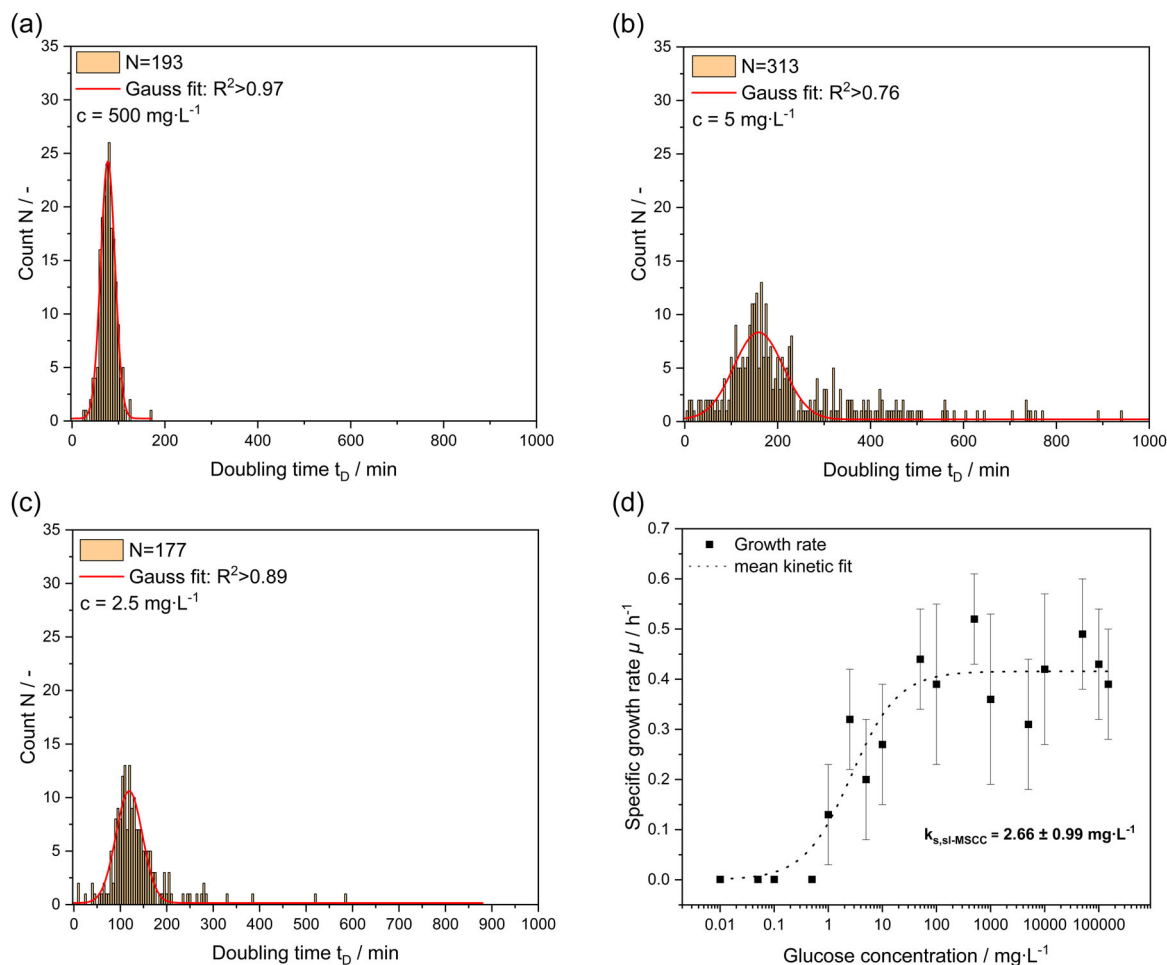
FIGURE 6 Cumulative distribution of t_D for at least three biological replicas containing at least 50 single-cell t_D of *Corynebacterium glutamicum* ATCC 13032 at (a) 500 mg/L, (b) 5 mg/L, (c) 2.5 mg/L glucose in CGXII. (d) Glucose-dependent maximum specific growth rates of individual *C. glutamicum* cells grown in microfluidic perfusion. The black line denotes the fit of the Monod equation to the data set.

limiting growth condition leads to a reduced energy availability for a subpopulation of cells which are struggling to maintain growth. It is reported that under limiting carbon-source conditions, cells have difficulties to maintain optimal growth and cell-to-cell heterogeneity increases (Bettenworth et al., 2019; Lindemann et al., 2019; Martins & Locke, 2015).

Therefore, single-cell t_D of at least three lineages of a mother cell were analyzed to determine μ. Within the observed glucose concentration range from 0 to 150 g/L, a Monod-type response was observed (Figure 6d). At concentrations higher than 500 mg/L, growth of *C. glutamicum* peaked and remained constant with an observed maximum specific growth rate of $\mu_{max} = 0.41 \pm 0.02\,h^{-1}$. At glucose concentrations between 1 mg/L and 100 mg/L an increase of doubling time was observed, resulting in reduced cell growth ($\mu = 0.13 \pm 0.10\,h^{-1}$, $\mu = 0.39 \pm 0.16\,h^{-1}$). Glucose concentrations smaller than 1 mg/L resulted in a growth arrest. The regression of the obtained growth data to the Monod equation yielded an average $k_{S,mean} = 2.66 \pm 0.99$ mg/L with a coefficient of determination of $R^2 = 0.87$.

3.3 | Comparison of k_S estimations

The presented methods within this work yielded comparable k_S values. Moreover, the obtained data are in good agreement with literature values (Table 1). The already published k_S values for glucose range from 0.52 to 7.68 mg/L, including given standard deviations. Lindner et al. (2011) obtained a value of 2.52 mg/L and Uhde et al. (2013) 2.17–2.70 mg/L by applying liquid scintillation counting. Both values match very well. However, the used protocol of both was highly similar. In these studies, different concentrations of ^{14}C labeled glucose was supplied to previously washed *C. glutamicum* cells. After defined time intervals, cell samples are collected and analyzed with a scintillation counter. The data indicate a high reproducibility and a very precise monitoring of glucose uptake rates. Nonetheless, the required equipment and components impede a broad and fast application of this method. In contrast, Graf et al. (2020) utilized enzymatic assays to determine glucose concentrations and deduct glucose consumption rates in batch and chemostat cultivations. Based on a mathematical fit, a k_S with 4.39 ± 3.20 mg/L

in batch and 0.97 ± 0.45 mg/L in chemostat cultivation has been estimated.

While an enzymatic assay for glucose has a detection limit of 400 µg/L, it provides an accurate and fast estimation of residual glucose concentration. However, if the expected affinity toward glucose is higher and consequently below the detection limit, liquid scintillation counting or HPLC are necessary. Interestingly, the authors note different k_S values for batch and chemostat cultivations but do not elaborate on the reason because the work had a different focus. This differentiation of batch and continuous cultivation for k_S value estimation is often neglected. However, the k_S value is subject to the cell state, duration of cultivation as well as environmental conditions and therefore, can vary between batch and chemostat cultivations. Reasons for the deviations could include the washout of slower growing cells due to the set dilution rate or the continuous supply of PCA as a secondary carbon source during chemostat cultivation (Bäumchen et al., 2007).

In addition to the aforementioned established methods, three alternative methods for k_S estimation are presented in this work. HFB and sl-RA are advantageous with their fast and, in the case of the sl-RA, simple estimation approach. Even though, the estimated k_S values suggest that sl-RA (8.55 ± 1.38 mg/L) and HFB (<70.7 mg/L with 95% probability) are not advisable for investigations below concentrations of 10 mg/L. For HFB, the temporal resolution of the BioLector-based biomass observations is limiting, at least for the presented application example with *C. glutamicum* and glucose as carbon source, resulting in a sharp switch from exponential to stationary phase growth. The increased k_S value for the sl-RA compared with the sl-MSCC method is partially explained by an inherent overestimation due to the measurement principle. Oxygen partial pressure values are averaged within the required measurement time frame for OTR determination. However, for the k_S estimation, the initial glucose concentrations are assumed. This effect becomes more prominent with further increased

lengths of the measurement phase (Supporting Information: S18). Similar to HFB, this overestimation depends on the sharpness of the switch from exponential to stationary phase and, therefore, on the k_S value. In contrast, a k_S value under defined environmental conditions was obtained by the sl-MSCC approach (2.66 ± 0.99 mg/L). This method is applicable in concentration ranges below 1 mg/L. The image acquisition frequency for determining t_D plays an essential role. A division event may be documented one frequency interval later than it occurred, leading to increased deviations of the determined t_D. This aspect is compensated by the number of individual cells tracked and counted. Therefore, the experimental and evaluation throughput of this method must be further increased. For initial estimations or situations where the k_S value is expected to be rather in the higher mg/L range, HFB and sl-RA can be taken into consideration due to the reduced labor intensity. The sl-MSCC method can yield similar results as lab-scale fermentations in combination with liquid scintillation counting or enzymatic assays. Moreover, sl-MSCC data contains additional information about cell-to-cell heterogeneities, which will be discussed in the following section.

3.4 | Potential of sl-MSCC

In contrast to the presented microtiter plate methods, sl-MSCC allows, in addition to k_S determination, insights into cell-to-cell heterogeneity regarding growth and t_D at different cultivation concentrations. For the assurance of a steady state during cultivation, the cumulative distribution of the t_D was plotted as a function of cell generation for each glucose concentration. Here, a constant distribution of the doubling time of approximately 80 min within the first 10 generations was observed for an applied concentration of 500 mg/L glucose (Figure 7a). Similar trends have been obtained for
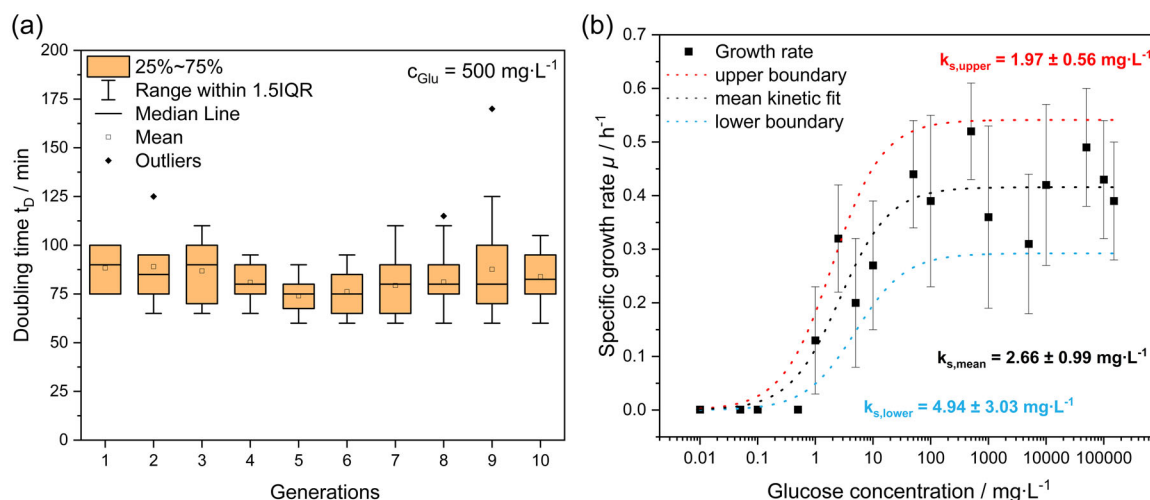

FIGURE 7 (a) Distribution of single-cell t_D of individual *Corynebacterium glutamicum* cells as a function of cell generations at a glucose concentration of 500 mg/L. (b) Glucose-dependent maximum specific growth rates of individual *C. glutamicum* cells grown in microfluidic perfusion. The black line denotes the fit of the Monod equation to the data set, while the red and blue lines give the upper and lower boundaries of the mathematical fit, respectively.

TABLE 1 Overview of substrate affinities of *Corynebacterium glutamicum* toward glucose.

Method	Analytics	k_S (mg/L)	Mode	Reference
[14]C uptake rate	Liquid scintillation counting	2.52	Batch	Lindner et al. (2011)
[14]C uptake rate	Liquid scintillation counting	2.17–2.70	Batch	Uhde et al. (2013)
Consumption rate	Enzymatic assay	4.39 ± 3.20	Batch	Graf et al. (2020)
Consumption rate	Enzymatic assay	0.97 ± 0.45	Chemostat	Graf et al. (2020)
HFB	BioLector	<70.7	Batch	This work
sl-RA	µTOM	8.55 ± 1.38	Batch	This work
sl-MSCC	Live-cell imaging	2.66 ± 0.99	Perfusion	This work

Abbreviations: HFB, high-frequency biomass; sl-MSCC, substrate-limited microfluidic single-cell cultivation; sl-RA, substrate-limited respiratory activity monitoring; µTOM, micro(µ)-scale Transfer rate Online Measurement.

other glucose concentrations, where steady-state growth lays the foundation for precise determination of t_D (Supporting Information: S1–S12). The first observation is that a steady state in cell growth and division at constant glucose concentrations of >1 mg/L can be maintained for at least 10 generations (up to the end of the experiment), which corresponds to <2 h/generation. At glucose concentration of ≤1 mg/L steady-state growth cannot be maintained for more than ~4.25 h/generation (Supporting Information: S13). Here, cell growth declines over the time course of cultivation, resulting even in a stop of growth after eight generations. A possible interpretation can be attributed to the declining storage of carbon sources (Farwick et al., 1995; Koch, 1983; Wolf et al., 2003). The obtained standard deviation, represented by the error bars in Figure 6d represents the cell-to-cell heterogeneity in t_D of the analyzed cells rather than a statistical error. Thus, 60% of the cells behave within the observed distribution of the average doubling time. This behavior can be used to determine upper and lower boundary values for k_S because these boundaries can be seen as an approximation of 95% of the cell behavior. Therefore, two additional mathematical fits were made to derive a k_S from the upper boundary (mean growth rate + standard deviation) and the lower boundary (mean growth rate − standard deviation). The mathematical fit of the estimated data yielded an upper boundary of $k_{S,upper\ boundary}$ = 1.97 ± 0.56 mg/L and a lower boundary of $k_{S,lower\ boundary}$ = 4.94 ± 3.03 mg/L with a statistical certainty of the applied regression to the Monod equation of R^2 > 0.92 for the upper boundary and R^2 > 0.73 for the lower boundary (Figure 7b).

In future, further sl-MSCC experiments need to show if and how cells adapt regarding growth and t_D at different concentrations. The emergence of potential subpopulations has to be analyzed (Arnoldini et al., 2014). These insights help to understand the cellular behavior at limiting conditions and, thus, the dynamics within k_S values.

The sl-MSCC method needs to be further parallelized, especially to collect statistically relevant numbers of cell division at limiting nutrient concentration ($c_S < k_S$). A critical step is progress in data analysis, which must be automated. In future, by an extension to an oscillation setup, k_S values under dynamic environmental conditions will be accessible, which cannot be measured with any other system (Ho et al., 2022).

4 | CONCLUSION

In this work, the recently introduced method of sl-MSCC, which enables the estimation of k_S by microfluidic perfusion experiments, was revisited and validated for the model organism *C. glutamicum* ATCC 13032 with glucose as limiting substrate and compared to HFB and sl-RA. Model-based Bayesian inference based on HFB is a rapid and extendible method to estimate the upper limits of k_S, where the possibility of estimating lower limits is directly dependent on the temporal resolution of the measurements. The sl-RA is an innovative and fast method that provides more precise values than HFB, because of the higher temporal resolution provided through online OTR measurement. However, for estimations of the k_S under defined environmental conditions, sl-MSCC in combination with live-cell imaging seems to be a superior technology because it provides insights into growth behavior at and below the substrate affinity, provides access to cell-lineage information and to single-cell heterogeneity. This enables to model a growth kinetic based on actual observed single-cell growth data without extrapolation. Additionally, sl-MSCC can be used to investigate the influence of cell-to-cell heterogeneity on bulk k_S values. The sl-MSCC gives insights into growth deviation and adaptation compared to HFB and sl-RA. In future, sl-MSCC may provide strain-specific k_S values to tackle the lack of availability. Furthermore, with the extension to an oscillation setup, affinities under fluctuating environmental conditions can be analyzed for the first time in future.

AUTHOR CONTRIBUTIONS

Conceptualization: Heiko Steinhoff and Alexander Grünberger. *Methodology*: Heiko Steinhoff, Maurice Finger, Michael Osthege, Simone Schito, Stephan Noack, Jochen Büchs, and Alexander Grünberger. *Formal analysis*: Heiko Steinhoff, Maurice Finger, Michael Osthege, Stephan Noack, Jochen Büchs, and Alexander Grünberger. *Investigation*: Heiko

ACKNOWLEDGMENTS

CONFLICT OF INTEREST STATEMENT

The authors declare no conflict of interest.

DATA AVAILABILITY STATEMENT

The data that support the findings of this study are available from the corresponding author upon reasonable request.

ORCID

Heiko Steinhoff https://orcid.org/0000-0003-0536-2134
Maurice Finger https://orcid.org/0000-0001-7384-8625
Stephan Noack http://orcid.org/0000-0001-9784-3626

REFERENCES

Arnoldini, M., Vizcarra, I. A., Peña-Miller, R., Stocker, N., Diard, M., Vogel, V., Beardmore, R. E., Hardt, W. D., & Ackermann, M. (2014). Bistable expression of virulence genes in salmonella leads to the formation of an antibiotic-tolerant subpopulation. *PLoS Biology*, *12*(8), e1001928. https://doi.org/10.1371/journal.pbio.1001928

Bäumchen, C., Knoll, A., Husemann, B., Seletzky, J., Maier, B., Dietrich, C., Amoabediny, G., & Büchs, J. (2007). Effect of elevated dissolved carbon dioxide concentrations on growth of *Corynebacterium glutamicum* on D-glucose and L-lactate. *Journal of Biotechnology*, *128*(4), 868–874. https://doi.org/10.1016/j.jbiotec.2007.01.001

Becker, J., Rohles, C. M., & Wittmann, C. (2018). Metabolically engineered *Corynebacterium glutamicum* for bio-based production of chemicals, fuels, materials, and healthcare products. *Metabolic Engineering*, *50*, 122–141. https://doi.org/10.1016/j.ymben.2018.07.008

Bettenworth, V., Steinfeld, B., Duin, H., Petersen, K., Streit, W. R., Bischofs, I., & Becker, A. (2019). Phenotypic heterogeneity in bacterial quorum sensing systems. *Journal of Molecular Biology*, *431*(23), 4530–4546. https://doi.org/10.1016/j.jmb.2019.04.036

Burmeister, A., Akhtar, Q., Hollmann, L., Tenhaef, N., Hilgers, F., Hogenkamp, F., Sokolowsky, S., Marienhagen, J., Noack, S., Kohlheyer, D., & Grünberger, A. (2021). (Optochemical) control of synthetic microbial coculture interactions on a microcolony level. *ACS Synthetic Biology*, *10*(6), 1308–1319. https://doi.org/10.1021/acssynbio.0c00382

Bylund, F., Collet, E., Enfors, S. O., & Larsson, G. (1998). Substrate gradient formation in the large-scale bioreactor lowers cell yield and increases by-product formation. *Bioprocess Engineering*, *18*(3), 171–180. https://doi.org/10.1007/s004490050427

Dinger, R., Lattermann, C., Flitsch, D., Fischer, J. P., Kosfeld, U., & Büchs, J. (2022). Device for respiration activity measurement enables the determination of oxygen transfer rates of microbial cultures in shaken 96-deepwell microtiter plates. *Biotechnology and Bioengineering*, *119*(3), 881–894. https://doi.org/10.1002/bit.28022

Enfors, S. O., Jahic, M., Rozkov, A., Xu, B., Hecker, M., Jürgen, B., Krüger, E., Schweder, T., Hamer, G., O'Beirne, D., Noisommit-Rizzi, N., Reuss, M., Boone, L., Hewitt, C., McFarlane, C., Nienow, A., Kovacs, T., Trägårdh, C., Fuchs, L., Manelius, Å. (2001). Physiological responses to mixing in large scale bioreactors. *Journal of Biotechnology*, *85*(2), 175–185. https://doi.org/10.1016/S0168-1656(00)00365-5

Farwick, M., Siewe, R. M., & Krämer, R. (1995). Glycine betaine uptake after hyperosmotic shift in *Corynebacterium glutamicum*. *Journal of Bacteriology*, *177*(16), 4690–4695. https://doi.org/10.1128/jb.177.16.4690-4695.1995

Ferenci, T. (1999). Growth of bacterial cultures' 50 years on: Towards an uncertainty principle instead of constants in bacterial growth kinetics. *Research in Microbiology*, *150*(7), 431–438. https://doi.org/10.1016/s0923-2508(99)00114-x

Freudl, R. (2017). Beyond amino acids: Use of the *Corynebacterium glutamicum* cell factory for the secretion of heterologous proteins. *Journal of Biotechnology*, *258*, 101–109. https://doi.org/10.1016/j.jbiotec.2017.02.023

Goudar, C. T., & Strevett, K. A. (1998). Estimating growth kinetics of *Penicillium chrysogenum* through the use of respirometry. *Journal of Chemical Technology & Biotechnology*, *72*(3), 207–212. https://doi.org/10.1002/(SICI)1097-4660(199807)72:3<207::AID-JCTB899>3.0.CO;2-B

Graf, M., Haas, T., Teleki, A., Feith, A., Cerff, M., Wiechert, W., Nöh, K., Busche, T., Kalinowski, J., & Takors, R. (2020). Revisiting the growth modulon of *Corynebacterium glutamicum* under glucose limited chemostat conditions. *Frontiers in Bioengineering and Biotechnology*, *8*, 584614. https://doi.org/10.3389/fbioe.2020.584614

Grünberger, A., Probst, C., Heyer, A., Wiechert, W., Frunzke, J., & Kohlheyer, D. (2013). Microfluidic picoliter bioreactor for microbial single-cell analysis: Fabrication, system setup, and operation. *Journal of Visualized Experiments: JoVE*, *82*, 50560. https://doi.org/10.3791/50560

Harrison, D. E. F. (1973). Studies on the affinity of methanol- and methane-utilizing bacteria for their carbon substrates. *Journal of Applied Bacteriology*, *36*(2), 301–308. https://doi.org/10.1111/j.1365-2672.1973.tb04106.x

Helleckes, L. M., Osthege, M., Wiechert, W., von Lieres, E., & Oldiges, M. (2022). Bayesian calibration, process modeling and uncertainty quantification in biotechnology. *PLoS Computational Biology*, *18*(3), e1009223. https://doi.org/10.1371/journal.pcbi.1009223

Hermann, T. (2003). Industrial production of amino acids by coryneform bacteria. *Journal of Biotechnology*, *104*(1–3), 155–172. https://doi.org/10.1016/S0168-1656(03)00149-4

Ho, P., Täuber, S., Stute, B., Grünberger, A., & von Lieres, E. (2022). Microfluidic reproduction of dynamic bioreactor environment based

on computational lifelines. *Frontiers in Chemical Engineering*, *4*, 826485. https://doi.org/10.3389/fceng.2022.826485

Ihling, N., Munkler, L. P., Berg, C., Reichenbächer, B., Wirth, J., Lang, D., Wagner, R., & Büchs, J. (2021). Time-resolved monitoring of the oxygen transfer rate of Chinese hamster ovary cells provides insights into culture behavior in shake flasks. *Frontiers in Bioengineering and Biotechnology*, *9*, 725498. https://doi.org/10.3389/fbioe.2021.725498

Junker, B. H. (2004). Scale-up methodologies for *Escherichia coli* and yeast fermentation processes. *Journal of Bioscience and Bioengineering*, *97*(6), 347–364. https://doi.org/10.1016/S1389-1723(04)70218-2

Kell, D. B., & Sonnleitner, B. (1995). GMP-good modelling practice: An essential component of good manufacturing practice. *Trends in Biotechnology*, *13*(11), 481–492. https://doi.org/10.1016/S0167-7799(00)89006-X

Koch, A. L. (1983). The surface stress theory of microbial morphogenesis. *Advances in Microbial Physiology*, *24*, 301–366. https://doi.org/10.1016/S0065-2911(08)60388-4

Kovárová-Kovar, K., & Egli, T. (1998). Growth kinetics of suspended microbial cells: From single-substrate-controlled growth to mixed-substrate kinetics. *Microbiology and Molecular Biology Reviews*, *62*(3), 646–666. https://doi.org/10.1128/MMBR.62.3.646-666.1998

Legan, J. D., & Owens, J. D. (1987). Determination of growth parameters of methylamine-using bacteria. *Microbiology*, *133*(4), 1075–1080. https://doi.org/10.1099/00221287-133-4-1075

Li, Y., Jin, M., O'Laughlin, R., Bittihn, P., Tsimring, L. S., Pillus, L., Hasty, J., & Hao, N. (2017). Multigenerational silencing dynamics control cell aging. *Proceedings of the National Academy of Sciences*, *114*(42), 11253–11258. https://doi.org/10.1073/pnas.1703379114

Liebl, W., Klamer, R., & Schleifer, K. H. (1989). Requirement of chelating compounds for the growth of *Corynebacterium glutamicum* in synthetic media. *Applied Microbiology and Biotechnology*, *32*(2), 205–210. https://doi.org/10.1007/BF00165889

Lindemann, D., Westerwalbesloh, C., Kohlheyer, D., Grünberger, A., & von Lieres, E. (2019). Microbial single-cell growth response at defined carbon limiting conditions. *RSC Advances*, *9*(25), 14040–14050. https://doi.org/10.1039/c9ra02454a

Lindner, S. N., Seibold, G. M., Henrich, A., Krämer, R., & Wendisch, V. F. (2011). Phosphotransferase system-independent glucose utilization in *Corynebacterium glutamicum* by inositol permeases and glucoki-nases. *Applied and Environmental Microbiology*, *77*(11), 3571–3581. https://doi.org/10.1128/AEM.02713-10

Mandenius, C.-F. (Ed.). (2016). *Bioreactors: Design, operation and novel applications* (1st ed.). Wiley-VCH. http://nbn-resolving.org/urn:nbn:de:bsz:31-epflicht-1081908

Martin, O., Hartikainen, A., Abril-Pla, C. O., Kumar, R., Gautam, P., Arroyuelo, A., Naeem, R., Banerjea, R. A., Pasricha, N., Gruevski, P., Sanjay, R., Rochford, A., Phan, D., Mahweshwari, U., Kazantsev, V., Arunava, Andorra, A., & Lozada, R. P. (2021). ArviZ. Zenodo.

Martins, B. M., & Locke, J. C. (2015). Microbial individuality: How single-cell heterogeneity enables population level strategies. *Current Opinion in Microbiology*, *24*, 104–112. https://doi.org/10.1016/j.mib.2015.01.003

Monod, J. (1949). The growth of bacterial cultures. *Annual Review of Microbiology*, *3*(1), 371–394. https://doi.org/10.1146/annurev.mi.03.100149.002103

Mühlmann, M. J., Forsten, E., Noack, S., & Büchs, J. (2018). Prediction of recombinant protein production by *Escherichia coli* derived online from indicators of metabolic burden. *Biotechnology Progress*, *34*(6), 1543–1552. https://doi.org/10.1002/btpr.2704

Oliveira, C. S., Ordaz, A., Alba, J., Alves, M., Ferreira, E. C., & Thalasso, F. (2009). Determination of kinetic and stoichiometric parameters of *Pseudomonas putida* F1 by chemostat and in situ pulse respirometry. *Chemical Product and Process Modeling*, *4*(2). https://doi.org/10.2202/1934-2659.1304

Ordaz, A., Oliveira, C. S., Aguilar, R., Carrión, M., Ferreira, E. C., Alves, M., & Thalasso, F. (2008). Kinetic and stoichiometric parameters estimation in a nitrifying bubble column through "in-situ" pulse respirometry. *Biotechnology and Bioengineering*, *100*(1), 94–102. https://doi.org/10.1002/bit.21723

Osthege, M., & Helleckes, L. M. (2022a). JuBiotech/calibr8: v6.4.0. Zenodo.

Osthege, M., & Helleckes, L. M. (2022b). JuBiotech/murefi: v5.1.0. Zenodo.

Osthege, M., & Schito, S. (2022). Supplement to Experimental k_S estimation: A comparison of methods for *Corynebacterium glutamicum* from lab to microfluidic scale. Zenodo.

Osthege, M., Tenhaef, N., Helleckes, L. M., & Müller, C. (2022). JuBiotech/bletl: v1.1.0. Zenodo.

Osthege, M., Tenhaef, N., Zyla, R., Müller, C., Hemmerich, J., Wiechert, W., Noack, S., & Oldiges, M. (2022). bletl - A Python package for integrating BioLector microcultivation devices in the Design-Build-Test-Learn cycle. *Engineering in Life Sciences*, *22*(3-4), 242–259. https://doi.org/10.1002/elsc.202100108

Phoenix, D. (1997). *Introductory mathematics for the life sciences. Modules in life sciences*. CRC Press.

Schindelin, J., Arganda-Carreras, I., Frise, E., Kaynig, V., Longair, M., Pietzsch, T., Preibisch, S., Rueden, C., Saalfeld, S., Schmid, B., Tinevez, J. Y., White, D. J., Hartenstein, V., Eliceiri, K., Tomancak, P., & Cardona, A. (2012). Fiji: An open-source platform for biological-image analysis. *Nature Methods*, *9*(7), 676–682. https://doi.org/10.1038/nmeth.2019

Schmieder, A., Severin, T. S., Cremer, J. H., & Weuster-Botz, D. (2015). A novel milliliter-scale chemostat system for parallel cultivation of microorganisms in stirred-tank bioreactors. *Journal of Biotechnology*, *210*, 19–24. https://doi.org/10.1016/j.jbiotec.2015.06.402

Senn, H., Lendenmann, U., Snozzi, M., Hamer, G., & Egli, T. (1994). The growth of *Escherichia coli* in glucose-limited chemostat cultures: A re-examination of the kinetics. *Biochimica Et Biophysica Acta (BBA)-General Subjects*, *1201*(3), 424–436. https://doi.org/10.1016/0304-4165(94)90072-8

Stöckmann, C., Maier, U., Anderlei, T., Knocke, C., Gellissen, G., & Büchs, J. (2003). The oxygen transfer rate as key parameter for the characterization of *Hansenula polymorpha* screening cultures. *Journal of Industrial Microbiology & Biotechnology*, *30*(10), 613–622. https://doi.org/10.1007/s10295-003-0090-9

Takors, R. (2012). Scale-up of microbial processes: Impacts, tools and open questions. *Journal of Biotechnology*, *160*(1–2), 3–9. https://doi.org/10.1016/j.jbiotec.2011.12.010

Täuber, S., Golze, C., Ho, P., von Lieres, E., & Grünberger, A. (2020). dMSCC: a microfluidic platform for microbial single-cell cultivation of *Corynebacterium glutamicum* under dynamic environmental medium conditions. *Lab on a Chip*, *20*(23), 4442–4455. https://doi.org/10.1101/2020.07.10.188938

ter Braak, C. J. F., & Vrugt, J. A. (2008). Differential evolution Markov chain with snooker updater and fewer chains. *Statistics and Computing*, *18*(4), 435–446. https://doi.org/10.1007/s11222-008-9104-9

Toepke, M. W., & Beebe, D. J. (2006). PDMS absorption of small molecules and consequences in microfluidic applications. *Lab on a Chip*, *6*(12), 1484–1486. https://doi.org/10.1039/b612140c

Uhde, A., Youn, J. W., Maeda, T., Clermont, L., Matano, C., Krämer, R., Wendisch, V. F., Seibold, G. M., & Marin, K. (2013). Glucosamine as carbon source for amino acid-producing *Corynebacterium glutamicum*. *Applied Microbiology and Biotechnology*, *97*(4), 1679–1687. https://doi.org/10.1007/s00253-012-4313-8

Unthan, S., Grünberger, A., van Ooyen, J., Gätgens, J., Heinrich, J., Paczia, N., Wiechert, W., Kohlheyer, D., & Noack, S. (2014). Beyond growth rate 0.6: What drives *Corynebacterium glutamicum* to higher growth rates in defined medium. *Biotechnology and Bioengineering*, *111*(2), 359–371. https://doi.org/10.1002/bit.25103

Vertès, A. A., Inui,M., & Yukawa, H. (2012). Postgenomic approaches to using corynebacteria as biocatalysts. *Annual Review of Microbiology*, *66*, 521–550. https://doi.org/10.1146/annurev-micro-010312-105506

von der Osten, C. H., Gioannetti, C., & Sinskey, A. J. (1989). Design of a defined medium for growth of *Corynebacterium glutamicum* in which citrate facilitates iron uptake. *Biotechnology Letters*, *11*(1), 11–16. https://doi.org/10.1007/BF01026778

Wang, P., Robert, L., Pelletier, J., Dang, W. L., Taddei, F., Wright, A., & Jun, S. (2010). Robust growth of *Escherichia coli*. *Current Biology*, *20*(12), 1099–1103. https://doi.org/10.1016/j.cub.2010.04.045

Wechselberger, P., Sagmeister, P., & Herwig, C. (2013). Real-time estimation of biomass and specific growth rate in physiologically variable recombinant fed-batch processes. *Bioprocess and Biosystems Engineering*, *36*(9), 1205–1218. https://doi.org/10.1007/s00449-012-0848-4

Wendisch, V. F., Bott, M., & Eikmanns, B. J. (2006). Metabolic engineering of *Escherichia coli* and *Corynebacterium glutamicum* for biotechnological production of organic acids and amino acids. *Current Opinion in Microbiology*, *9*(3), 268–274. https://doi.org/10.1016/j.mib.2006.03.001

Wendisch, V. F., Jorge, J., Pérez-García, F., & Sgobba, E. (2016). Updates on industrial production of amino acids using *Corynebacterium glutamicum*. *World Journal of Microbiology & Biotechnology*, *32*(6), 105. https://doi.org/10.1007/s11274-016-2060-1

Wiecki, T., Salvatier, J., Patil, A., Kochurov, M., Engels, B., Lao, J., Colin Martin, O., Ricardo, V., Willard, B. T., & Osthege, M. (2022). pymc-devs/pymc: v4.0.0b2. Zenodo.

Wolf, A., Krämer, R., & Morbach, S. (2003). Three pathways for trehalose metabolism in *Corynebacterium glutamicum* ATCC13032 and their significance in response to osmotic stress. *Molecular Microbiology*, *49*(4), 1119–1134. https://doi.org/10.1046/j.1365-2958.2003.03625.x

SUPPORTING INFORMATION

Additional supporting information can be found online in the Supporting Information section at the end of this article.